Chlorin e6-loaded ethosomes for photodynamic wound therapy

Nina A. Kalyagina[1,2]*, Artem A. Shiryaev[3], Oleg S. Kudryavtsev[1], Dmitry V. Yakovlev[1], Mikhail P. Ivankov[3], Aleksey S. Skobeltsin[1], Alim F. Malikov[2], and Victor B. Loschenov[1,2]

ABSTRACT

Improving and optimizing photosensitizers for photodynamic wound therapy remains an urgent task in this field. This study investigates the properties of an ethosomal chlorin e6 (Ce6) photosensitizer and its penetration into various tissues within a wound area. We obtained and analyzed spatial- and geometric configurations, absorption and fluorescence spectra of Ce6 in both molecular and ethosomal forms, alongside studying its penetration into skin and muscle tissue. The synthesized particles were spherical with convex surfaces. The average particle diameter in the samples was 47.7 nm. The absorption and fluorescence spectra of ethosomal Ce6 exhibited a bathochromic shift of 13–16 nm relative to molecular Ce6. This shift in the fluorescence peak was primarily attributed to the presence of lecithin in the ethosomal solution. In contrast, the variability in peak position along the wavelength axis (2–5 nm) was more likely due to ethanol in the solution. Encapsulation of Ce6 in ethosomes overcomes the stratum corneum barrier of the skin, providing 1.5- to 2-fold deeper penetration (up to 180 μm) into the epidermis and papillary dermis compared to free Ce6 (50–120 μm). Upon direct application to muscle tissue, which lacks an epithelial barrier, both formulations penetrate substantially deeper (up to 1500 μm for ethosomal Ce6); however, tissue heterogeneity introduces considerable variability. Therefore, when planning diagnosis or therapy using ethosomal Ce6, it is necessary to select irradiation sources with wavelengths corresponding to these new, shifted absorption peaks, along with appropriate filters for detecting fluorescence in the new spectral range. Furthermore, the potentially greater and more variable depth of tissue saturation compared to skin must be taken into account, as this is a decisive factor in determining the optimal parameters for laser or light-emitting diode irradiation.

Keywords:

Antimicrobial photodynamic therapy; Chlorin e6; Ethosomes; Wound; Fluorescence

***Corresponding author:**
Nina A. Kalyagina,
nina.kalyagina@gmail.com

How to cite this article:
Kalyagina NA, Shiryaev AA, Kydryavtsev OS, *et al.* Chlorin e6-loaded ethosomes for photodynamic wound therapy. *Biomater Transl.* 2026, 7(2), 321-328.

doi: 10.12336/bmt.25.00177

1. Introduction

Photodynamic therapy (PDT) is a technique that involves the introduction or application of a photosensitizing agent (photosensitizer [PS]), followed by irradiation of the target tissue with light at specific wavelengths, for cancer treatment, wound healing, and other applications. The mechanism of action of PDT is based on the use of PS and light to form cytotoxic reactive oxygen species and subsequent oxidation of tissue (in the case of a tumor) or bacteria (in the case of infected wounds) exposed to light, as well as the initiation of local response mechanisms followed by an immune response or tissue regeneration (for wound healing).

Effective delivery of PS to target sites to eliminate bacteria and initiate regenerative processes is a challenging task in wound healing. Conventional PSs remain far from ideal due to their poor permeability, side effects, hydrophobicity, poor bioavailability, and tendency to self-aggregate.[1] This fact, combined with the fact that numerous PSs are small and hydrophobic, has led to the widespread study of approaches to nanoscaling

and encapsulating PSs to develop more effective delivery vehicles.[2,3]

PSs can be encapsulated in liposomes, a well-known PS delivery vehicle that is a spherical vesicle consisting of one or more phospholipid bilayers (lamellae) organized around an internal aqueous core, with polar head groups oriented toward the internal and external aqueous phases.[4] Such an organized structure can provide liposomes with the unique ability to load and deliver both hydrophobic and lipophilic agents.[5,6]

Currently, lipid-based nanomedicines are being studied and used for targeted drug delivery to the target site, protection of drugs from *in vivo* degradation, control of drug release, alteration of biodistribution, enhancement of solubility and bioavailability, and as vaccine adjuvants due to their ability to protect and deliver antigens (peptide, protein, and nucleic acid systems) to antigen-presenting cells, and stimulate protective immune responses.[7] For example, liposomes can improve the therapeutic efficacy of drugs/PS by stabilizing the compounds, overcoming barriers to cellular and tissue absorption, and increasing the biodistribution of drugs to target sites *in vivo*, while being non-toxic, biocompatible, and biodegradable.[5,8] In studies for PDT in oncology, liposomes have been shown to offer various benefits, such as increasing selectivity, reducing side effects, reducing immunogenicity, and increasing phototoxicity of PS, thereby providing higher PDT efficiency.[1] Furthermore, using liposomes to encapsulate PS in their hydrophobic bilayer or aqueous core is a relatively simple approach. Several liposomal PS formulations have shown great potential for effective *in vivo* PDT, but a strong tendency to aggregate in aqueous solution has been identified, resulting in poor bioavailability and limited tissue penetration.[1]

In addition to liposomes, ethosomal nanoparticles can help overcome the limitations of PDT. Ethosomes, descendants of liposomes, are nanovesicular systems composed of phospholipids and ethanol.[9] These formulations were developed to overcome the insufficient penetrating ability of traditional liposomes, which deliver drugs to the superficial layers of the skin rather than to the deep layers.[10] Ethosomes have a smaller vesicle size and greater stability compared to conventional liposomes. In addition, their distinctive advantages of non-toxicity and non-irritability have attracted the attention of numerous researchers.[11,12] Compared to liposomes, ethosomal systems use a high ethanol concentration, ranging from 20% to 50% in the formulation.[13,14] Ethanol is a known permeation enhancer that imparts unique properties to ethosomes, including high elasticity and deformability, enabling deep penetration into the skin and enhancing the penetration and deposition of drugs. The improved composition of ethosomes thus provides significant advantages for the delivery of therapeutic agents, particularly compared to conventional liposomes, across various pathologies.[14,15] In this regard, the current study aims to study the properties of ethosomal PS and their penetration into the wound area using chlorin e6 (Ce6).

2. Methods

2.1. Ethosomal solutions

Nanocomposites of Ce6 were synthesized as follows: at a temperature of 30°C, bidistilled water was slowly added in a thin stream to pure egg yolk lecithin (Serva, Germany) and PS (Fotoran e6; OOO DEKO, Russia), dissolved in ethanol, with constant stirring at a speed of 700 rpm using a laboratory blender (MSH-300, Biosan, Latvia) for 5 min. The resulting dispersion was extruded through a 0.22 μm polytetrafluoroethylene syringe filter. The ethosomal system was then cooled to room temperature. The concentrations of Ce6 in the studied molecular and ethosomal solutions were adjusted to 0.1 mg/mL. Ethosomal solutions, separately with ethanol or lecithin, were prepared similarly with (or without) the corresponding components. The method of application and the effectiveness of treatment using such and similar ethosomal solutions have been previously studied.[16,17]

The amount of PS encapsulated in the ethosomes was assessed by determining the encapsulation efficiency (EE) and the loading capacity (LC). To separate free (non-encapsulated) Ce6 from the ethosome-encapsulated fraction, an ultrafiltration method was employed. A 400 μL aliquot of the ethosome suspension was placed into a 100 kDa centrifugal filter device. Primary centrifugation was carried out for 20 min at 10,000 × g. The resulting filtrate (Fraction 1) was collected. The volume of the retentate was reconstituted to the initial 400 μL using a hydroalcoholic solution, after which the centrifugation procedure was repeated under the same conditions (20 min, 10,000 × g). This yielded a second filtrate (Fraction 2). The concentration of free Ce6 was determined spectrophotometrically in the combined filtrates. The calculations of EE and LC were performed according to the following equations (Equations 1 and 2):

$$EE(\%) = \frac{A_0 - A_u}{A_0} \times 100 \quad (1)$$

$$LC(\%) = \frac{A_0 - A_u}{W} \times 100 \quad (2)$$

where A_0 is the total (initial) amount of the PS used in the formulation; A_u is the amount of free (unencapsulated) PS remaining in the solution after ethosome separation, and W is the mass of the lecithin.

[1]Department of Light-Induced Surface Phenomena, Natural Sciences Center, Prokhorov General Physics Institute of the Russian Academy of Sciences, Moscow, Russia; [2]Department of Laser Micro-Nano and Biotechnology, Institute for Physics and Engineering in Biomedicine, National Research Nuclear University MEPhI, Moscow, Russia; [3]Department of Oncology, Radiotherapy and Reconstructive Surgery, L.L. Levshin Institute of Cluster Oncology, Sechenov First Moscow State Medical University (Sechenov University), Moscow, Russia

2.2. Spatial and geometric configuration and absorption and fluorescence spectra of Ce6 in molecular and ethosomal forms

The study of particles using atomic force microscopy (AFM) requires applying particles from a colloidal solution onto a flat, solid substrate. The ideal substrate for this case is a silicon wafer, the working surface of which was formed by precision polishing, followed by epitaxial growth of the finishing layer. The roughness of such a substrate is sufficiently low to enable the detection of individual particles within the expected size range. The particles were applied to the substrate using the vacuum seeding method.[18] This technology allows depositing particles from colloidal solutions onto the substrate surface, avoiding particle aggregation during solvent evaporation. Before seeding the particles onto the substrate, the solution was diluted 10 times with ethyl alcohol to prevent particle aggregation and additional rarefaction during seeding, simplifying the study of the particles using AFM. After diluting the solution, it was treated in an ultrasonic bath to homogenize and break down aggregates. The ultrasonic treatment time was 40 s. Such a short treatment time is due to the particles' low mechanical strength. The solution (10 μL) was then applied onto the substrate using a micropipette, and the substrate was placed in a vacuum chamber. After the chamber was closed, it was evacuated to remove the solvent through freeze-drying. When the pressure in the chamber was reduced to 0.1 Torr, the evaporation time of a drop of solution was approximately 2 s. After the solvent evaporated, the chamber was gradually ventilated, and the pressure was returned to atmospheric pressure over 5 min. The low ventilation rate of the chamber was required to minimize airflow and prevent particles from falling off the surface. Then the substrate with the particles seeded on it was placed under a microscope for examination.

Measurements of the sample's spatial configuration, particle morphology, and particle fluorescence-spectrum registration were performed using the NTEGRA Spectra Probe Nanolaboratory (nanotechnology-molecular devices and tools [NT-MDT], NT-MDT Spectrum Instruments, Russia). Ethosomes were seeded onto a silicon substrate using a unique vacuum method. A medium vacuum was created in the chamber to remove moisture, with a pressure of 0.2 Torr maintained. This seeding method allowed rapid solvent evaporation without heating to the boiling point, which would have destroyed the ethosomes. The alternative method of prolonged solvent evaporation at room temperature was unsuitable in our case, as it caused the ethosomes to aggregate heavily, forming large agglomerates composed of numerous particles, which limited the study of individual objects.

Visualization of the surface, focusing of the exciting laser radiation, and collection of the useful fluorescence and Raman scattering signals were carried out using a Mitutoyo objective with ×100 magnification, a numerical aperture of 0.65, and a working distance of 10 mm. In addition, the system enabled measurements of the sample surface topography and morphology using atomic force and scanning tunneling microscopy with nanometer resolution. Using this system, 2D and 3D spatial and geometric configurations of the Ce6 ethosomes were obtained.

Visible absorption spectra (optical density) were recorded using a spectrophotometer (HITACHI). Two quartz cuvettes with an optical path length of 1 cm were used as sample and reference holders. Distilled water was used as a universal reference solution, providing a correction for the cuvette and solvent background absorption. First, a baseline was established by filling both cuvettes with distilled water to the same level, ensuring identical optical paths. To assess the absorption contributions of the cuvette and solvent materials, as well as background noise, the cuvette containing distilled water was placed in the instrument holder, after which the baseline spectrum was recorded and subtracted from subsequent measurements. The prepared ethosomal solution was diluted 200-fold. The water was then drained from the measuring cuvette, the cuvette was rinsed with a small volume of the ethosomal solution, and then completely filled with the solution. The sample cuvette was placed in the holder with the same spatial orientation as the control cuvette during calibration. The optical density spectrum of the ethosomal solution was then measured.

2.3. Penetration depth of molecular and ethosomal forms of PS into various tissue types

2.3.1. Patients and skin model

Studies on the penetration depth of Ce6 in molecular and ethosomal forms were conducted on muscle biopsy samples of a patient with a wound of the left thigh (traumatic amputation), as well as on biopsy samples of skin and muscle tissue of biological tissue *ex vivo* (chicken) (five samples of each type, skin and muscle). The patient was treated at the Clinical Center of the First Moscow State Medical University named after I. M. Sechenov, and biopsy specimens were obtained during tissue resection to close the wound defect. *Ex vivo* biological tissue was commercially purchased within 24 h of the animal's death and transported to the laboratory in a refrigerator at 4°C.

2.3.2. Penetration depth of the PS in biopsy material

The biopsy material was obtained from the wound after PS application through irrigation before PDT. The material was placed in a 0.9% physiological solution, after which it was delivered to the laboratory for examination. Localization of Ce6 in tissues was determined via fluorescence using a laser scanning confocal microscope (LSM-710-NLO, Carl Zeiss Microscopy, Germany). For this purpose, the obtained tissue pieces measuring 5 × 5 mm were frozen without preliminary fixation in an optimal cutting temperature compound for subsequent processing into 20 μm thick sections using a freezing microtome (Microm HM 560, MICROM International GmbH, Germany). Tissue autofluorescence was excited with a 488 nm laser, and emission was collected at 500–600 nm (green channel). Ce6 fluorescence was excited with a 633 nm laser, and registration was conducted in the range of 650–750 nm (red channel). Autofluorescence and Ce6 fluorescence were recorded in parallel. The concentration of Ce6 was estimated from the red-channel signal intensity.

3. Results

3.1. Spatial and geometric configuration of ethosomes

The amount of PS encapsulated in the ethosomes was determined to be 86% and 0.86% for EE and LC, respectively. On the AFM, the obtained ethosomes (a total of 56 images, 1–32 ethosomes in each image) of Ce6 are particles of a round shape with a convex surface (**Figure 1A** and **B**). After the initial image processing, which brought the data to a single level by subtracting the mean plane, two profiles were constructed for each ethosome in each image: along the X- and Y-axes, from which the metric data for the studied particles were calculated. The obtained particle profiles along the X- and Y-axes reveal minimal differences between measurements. Using the *t*-criterion, it was determined that there are no statistically significant differences between the measurements along the X- and Y-axes (p=0.05). Further in the work, the particle sizes in the XY plane will be defined as the average of the vertical and horizontal components.

Relative particle height profiles were also obtained and analyzed (**Figure 1C**). According to AFM, the particle heights ranged from 2 to 70 nm, even for large particles. The average particle diameter in the obtained samples, determined by dynamic light scattering (DLS), was 47.7 nm (**Figure 2**). In AFM images, the ethosomes appear significantly larger along the X- and Y-axes than their average size determined by DLS. This fact is attributed to the possible formation of flat particle aggregates during the complex, multi-step sample preparation procedure, as well as to the specific design of the measuring probe, which features a pyramidal shape with an apex angle of approximately 30° and a tip curvature radius of about 10 nm. Image reconstruction does not account for the probe's geometry, as the software always models it as a thin, long needle. Consequently, the probe's side begins to influence the measurement results. As the probe approaches an ethosome, its side contacts the particle much earlier than the tip, whose position determines the image being constructed. Therefore, the resulting image of the ethosome is reconstructed to a larger area. However, when the probe passes over the apex of the ethosome, it interacts with it precisely at the tip. Thus, the resulting images are significantly distorted horizontally but are more accurate vertically due to the probe's geometry. Nevertheless, a cross-sectional analysis shows that ethosome height is somewhat smaller than their average size measured by DLS. This is also explained by the probe-ethosome interaction. Since the ethosome is elastic, it may undergo slight deformation on contact with the probe tip.

3.2. Absorption spectra of Ce6 in molecular and ethosomal forms

A bathochromic shift was observed in the absorption spectra of ethosomal Ce6. The absorption maximum of "classical" Ce6 in the red region shifted toward longer wavelengths by approximately 14 nm for the ethosomal form (**Figure 3**). At the same time, the absorption intensity decreased with ethosomes. These features should be taken into account when prescribing

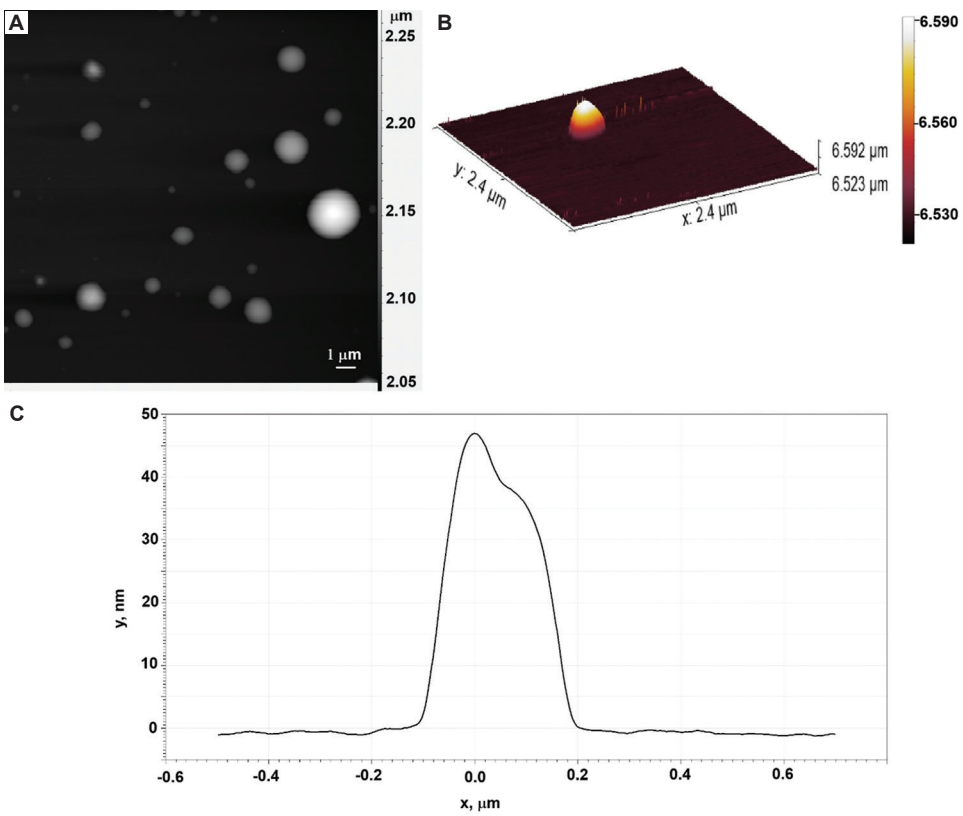

Figure 1. Visualization of ethosomes. (A) Example of a two-dimensional image with ethosomes. (B) Three-dimensional visualization of a single ellipsoidal shape of Ce6 ethosome in pseudo-colors. (C) Height profile of the Ce6 ethosome shown in (B).
Abbreviation: Ce6: Chlorin e6.

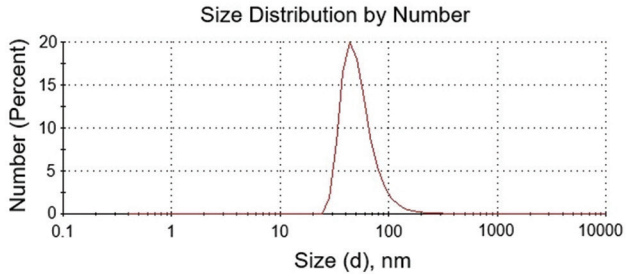

Figure 2. Distribution of particle sizes (average hydrodynamic radius).

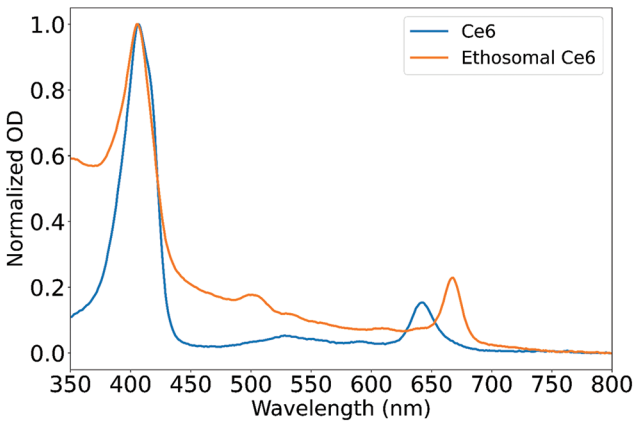

Figure 3. Absorption spectra of chlorin e6 in molecular and ethosomal forms.
Abbreviation: OD: Optical density.

and selecting the drug dosage, irradiation wavelengths, and light dose for PDT.

3.3. Fluorescence spectra of ethosomal Ce6

The obtained fluorescence spectra of Ce6 in the ethosomal form show a shift of the maximum toward longer wavelengths by 13–16 nm relative to the fluorescence spectra of Ce6, as well as instability in the position of the fluorescence maximum in the range from 673 to 676 nm (**Figure 4**). This effect is caused by the presence of impurity components in the initial solution of PS. The fluorescence intensities of ethosomal and molecular Ce6 did not differ statistically significantly (p>0.05).

To study the influence of individual impurities (ethanol and lecithin) on the fluorescence signal, the fluorescence spectra of ethosomal solutions of Ce6 were analyzed under these conditions: (i) Without lecithin, with ethanol, (ii) without ethanol, with lecithin, and (iii) in the classical form with ethanol and lecithin (**Figure 4**).

The absence of ethanol does not contribute to the fluorescence signal of the ethosomes: the fluorescence peak remains shifted toward longer wavelengths relative to Ce6 and matches the peak and spectrum shape of the "classic" ethosomes. In contrast, the PS in ethanol without lecithin produces a completely different spectral shape, with a main peak that is unstable and shifted toward shorter wavelengths, and an additional peak in the 730–735 nm region. Such data indicate that the main shift

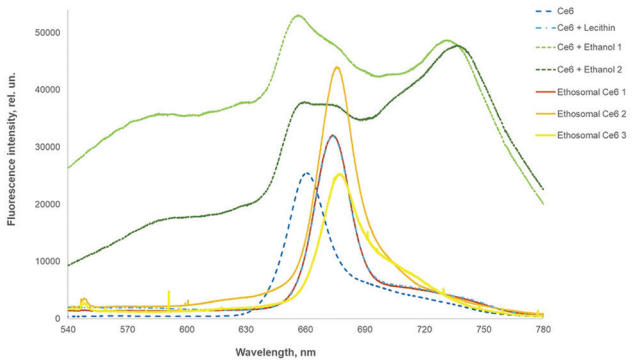

Figure 4. Fluorescence spectra of Ce6 with various components added separately: Ce6 alone, Ce6 with lecithin, Ce6 with ethanol, and ethosomal Ce6, showing an unstable shift in the peak position.
Abbreviation: Ce6: Chlorin e6.

of the fluorescence peak along the wavelength scale occurs due to the presence of lecithin in the ethosome solution. In contrast, the unstable position of the peak along the wavelength axis (with a spread of 2–5 nm) is more likely attributable to ethanol in the solution.

The observed instability in the fluorescence maximum position of the PS in the presence of ethanol, without a clear dependence on ethanol concentration, is most likely due to changes in the dye's microenvironment and in the dynamics of energy-relaxation processes. Since fluorescence is sensitive to the polarity and viscosity of the microenvironment, the addition of ethanol alters the solvation shell of the PS molecules and affects the emission. Ethanol, possessing a dipole moment and the ability to form hydrogen bonds, creates local heterogeneities in the solvent distribution around the fluorophore. In this case, ethanol molecules may interact specifically with heteroatoms or polar groups on the sensitizer, thereby shifting energy levels. The instability of the maximum is probably due to competition among two or more distinct types of solvation complexes or conformers of the PS, which are in dynamic equilibrium.

The lack of a clear relationship with ethanol concentration may be explained by the fact that once a sufficient number of ethanol molecules surround the PS molecule to form the first solvation shell or to establish an equilibrium between "bound" and "free" states, a further increase in the bulk ethanol concentration does not fundamentally alter the local structure of the fluorophore's immediate environment. In other words, the system transitions into a regime where fluctuations are caused not by the amount of ethanol, but by its dynamics—namely, the reorientation of dipoles and the breaking/formation of hydrogen bonds in the immediate vicinity of the chromophore. These processes are stochastic and can result in signal instability. Thus, the instability of the maximum is a consequence of the dynamic heterogeneity of the medium created by the ethanol, where the key role is played by the very presence of a strong local perturbing factor (dipole molecules), rather than their total quantity in the solution, at least within the range of concentrations studied.

3.4. Penetration depth of molecular and ethosomal forms of PS into various tissues

The high barrier function of the skin, particularly the stratum corneum rich in keratin and lipids, significantly restricts the passive diffusion of hydrophilic molecules such as Ce6. Upon topical application, free Ce6 is, in most cases, limited to penetrating the stratum corneum, with only trace amounts potentially reaching the deeper epidermal layers. Encapsulation of Ce6 in ethosomes enables deeper skin penetration. The ethanol present in the formulation transiently fluidizes the lipid bilayers of the stratum corneum, increasing its permeability, while the plasticity of the vesicles allows them to navigate intercellular channels and reach the deeper layers of the epidermis and dermis. In intact skin, free Ce6 was detected at average depths of 85.3 ± 42.4 μm (**Figure 5**, $p<0.05$, *t*-test), whereas ethosomal Ce6 reached depths of 115.2 ± 65.7 μm ($p<0.05$, *t*-test). It was found that the ethosomal formulation penetrated 1.5–2-fold deeper than the molecular form, reaching the epidermal layer and the papillary dermis.

In contrast, upon direct application to exposed muscle tissue (e.g., in a wound), the epithelial barrier is absent. The formulation is applied to a surface covered only by a thin, non-obstructive fascia. Free Ce6, as a low-molecular-weight compound, rapidly diffuses into the interstitial space, distributing among the muscle fibers. Muscle tissue, including infected variants, lacks a multilayered epithelial covering and has a loose connective tissue stroma (comprising the endomysium and perimysium) and an extracellular matrix that presents substantially lower diffusional resistance than the dense, keratinized structures of the skin. Although the full thickness of the muscle is accessible to penetration, the effective depth achieved by passive diffusion is uneven compared to that achieved with systemic administration via the bloodstream. In exposed muscle tissues, the penetration depth ranged from 100 to 500 μm for free Ce6 and up to 1500 μm for the ethosomal formulation. The wide variability in muscle tissue penetration is attributed to tissue heterogeneity combined with the absence of barriers present in the skin. When applied to muscle tissue, ethosomes likely retain the PS within their membranes and prolong its release into the interstitium, resulting in a high local concentration (**Figure 6**). Due to this heterogeneity, we were unable to establish a statistically significant numerical difference in penetration depth between the two formulations in muscle tissue across our samples. However, in some cases, such as in infected muscle, a pronounced difference in penetration depth—up to a 5-fold advantage for the encapsulated form—was observed (**Figure 6**).

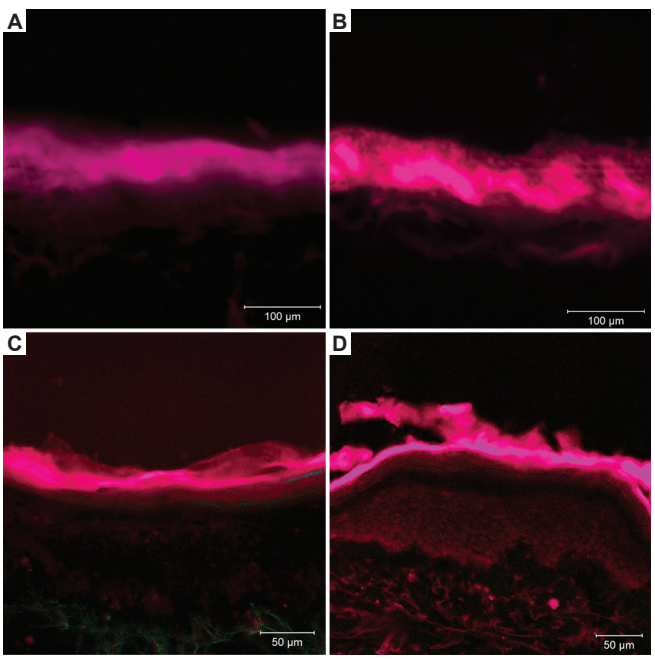

Figure 5. Fluorescence microscopy images of skin biopsy sections with PS. (A) Chicken skin 10 min after topical application of Ce6. Scale bar: 100 μm. (B) Chicken skin 10 min after topical application of ethosomal Ce6. Scale bar: 100 μm. (C) Human leg skin 10 min after topical application of Ce6. Scale bar: 50 μm. (D) Human leg skin 10 min after topical application of ethosomal Ce6. Scale bar: 50 μm. Pink coloration indicates PS fluorescence at depth.
Abbreviations: PS: Photosensitizers, Ce6: Chlorin e6.

4. Discussion

Ethosomal Ce6 shows an unstable position of the fluorescence maximum in the red wavelength range, with a shift of 4 nm in wavelength. This phenomenon is associated with impurities in the solution. However, since video recording devices with either long-pass or wide-band filters, which leave a large range for obtaining a fluorescence signal in the range of about 650–700 nm, are mainly used to monitor the treatment of wound surfaces using PDT, it can be concluded that these shifts in the maximum position will not affect the detection of the fluorescence signal during diagnostic monitoring of PDT.

Shifts in the absorption maxima of the ethosomal Ce6 are important for laser irradiation, since the laser spectral line is narrow and must be taken into account when selecting a radiation source for therapy or diagnostics, as well as when selecting filters for fluorescence visualization. Light-emitting diode radiation sources, whose spectral width can be as narrow as 30 nm, can offer fewer difficulties and greater versatility. In addition, the absorption characteristics of ethosomal solutions (bathochromic shift and intensity) should be considered when selecting the drug dose, irradiation wavelengths, and light dose for PDT.

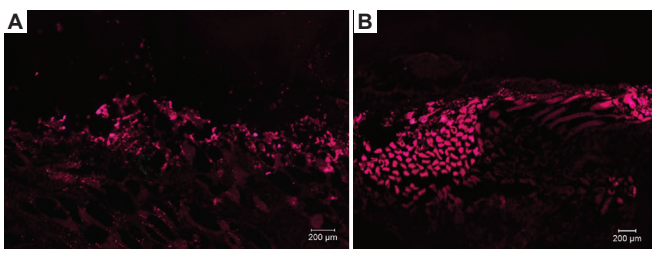

Figure 6. Fluorescence microscopy images of infected muscle tissue biopsy sections with PS. (A) Human leg muscle tissue 10 min after topical application of Ce6. Scale bar: 200 μm. (B) Human leg muscle tissue 10 min after topical application of ethosomal Ce6. Scale bar: 200 μm. Pink coloration indicates PS fluorescence at depth.
Abbreviations: PS: Photosensitizers, Ce6 chlorin e6.

The difference in the penetration depth of PS in the molecular and ethosomal forms into the skin is explained by the fact that ethosomes are PS carriers with lipid bilayers composed of phospholipids, water, and ethanol, which enhance transdermal permeability. Ethanol and lipid molecules act in the polar head region, increasing membrane fluidity and permeability.[19] Ethanol reduces the size of vesicles and generates a negative charge, which liquefies both vesicles and skin lipids and improves skin permeability for ethosomes.[20] Typically, ethosomes improve delivery through the skin, transferring active compounds to deeper layers of the skin under occlusive and non-occlusive conditions.[19] To improve the penetration of PS into muscle tissue, as well as to increase the overall depth of penetration of PS into tissue, novel formulations should be developed in the future.

For muscle tissue, which lacks an epidermal covering, the penetration depth of the PS upon topical application through spraying is limited only by the superficial fascia and the PS's diffusion capacity. Furthermore, the absence of an epidermal barrier and the specific organization of the connective tissue framework in muscles allow Ce6 to penetrate significantly deeper than in skin.

Deeper diffusion of ethosomal solutions of the used PSs into the skin promotes the occurrence of a photochemical reaction in deeper layers of the wound surface. In this regard, it is proposed to use ethosomal forms of PSs in future studies. To enhance the penetration of Ce6 into muscle tissue, additional methods can be considered, such as pulsed high-intensity focused ultrasound,[21] pulsed electric field,[22] and strict control of particle sizes,[23] to increase the penetration depth of various PS, ethosomal, and other nanoparticles. However, during treatment selection, the method should take into account the possibility of pain in open muscle tissue in the wound and the need for sterility during manipulations.

5. Conclusions

In this work, the spatial structure of Ce6 ethosomes was obtained and characterized for the 1st time. In addition, the absorption and fluorescence spectra of Ce6 and ethosomal Ce6 were recorded and analysed, leading to the conclusion that when planning diagnosis and therapy using ethosomal Ce6, it is necessary to select radiation sources with wavelengths corresponding to the "new" (shifted) absorption peaks relative to molecular Ce6, as well as filters for detecting fluorescence emission in the new wavelength range. Furthermore, due to the deeper penetration of Ce6 into the skin, the ethosomal formulation may offer an advantage over the conventional molecular form and could be used to treat wound edges, where the skin remains intact, and the most problematic areas for healing are often located. However, the barrier properties of the multilayered, keratinized squamous epithelium of the skin largely confine the PS's action to the epidermal layers and the upper dermis. In contrast, the absence of an epidermal barrier and the specific organization of the connective tissue framework in muscles allow the substance to penetrate much deeper. This indicates that when planning PDT for open wounds or muscle surfaces, the potentially greater and more variable depth of tissue saturation compared to skin must be taken into account, as this is a decisive factor in determining the optimal parameters for laser/light-emitting diode irradiation.

Acknowledgement
None.

Financial support
This study was funded by the Russian Science Foundation grant (No. 22-72-10117-П, https://rscf.ru/project/22-72-10117-П/).

Conflicts of interest statement
The authors declare that they have no corporate or financial affiliations that could be interpreted as a potential conflict of interest.

Author contributions
Conceptualization: VL, NK, and AAS; *Formal analysis:* NK and DY; *Investigation:* OK, MI, ASS; *Methodology:* OK, MI, DY, and ASS; *Project administration:* VL and AAS; *Writing–original draft:* NK, OK, and AM; *Writing–review & editing:* VL and AAS. All authors have read and agreed to the final manuscript.

Ethics approval and consent to participate
This study was reviewed and approved by the Ethics Committee of I.M. Sechenov First Moscow State Medical University (Sechenov University) (protocol code 13–22 from January 20, 2022). Informed consent was obtained from all patients.

Consent for publication
All participants provided informed consent for the publication of the findings derived from this study.

Availability of data
All data supporting the findings of this study are available within the paper. No additional external data sources were used.

References

1. Moghassemi S, Dadashzadeh A, Azevedo RB, Feron O, Amorim CA. Photodynamic cancer therapy using liposomes as an advanced vesicular photosensitizer delivery system. *J Control Release.* 2021;339:75-90. doi: 10.1016/j.jconrel.2021.09.024
2. Bechet D, Couleaud P, Frochot C, Viriot ML, Guillemin F, Barberi-Heyob M. Nanoparticles as vehicles for delivery of photodynamic therapy agents. *Trends Biotechnol.* 2008;26(11):612-621. doi: 10.1016/j.tibtech.2008.07.007
3. Ghosh S, Carter KA, Lovell JF. Liposomal formulations of photosensitizers. *Biomaterials.* 2019;218:119341. doi: 10.1016/j.biomaterials.2019.119341
4. Nisini R, Poerio N, Mariotti S, De Santis F, Fraziano M. The multirole of liposomes in therapy and prevention of infectious diseases. *Front Immunol.* 2018;9:155. doi: 10.3389/fimmu.2018.00155
5. Sebaaly C, Greige-Gerges H, Stainmesse S, Fessi H, Charcosset C. Effect of composition, hydrogenation of phospholipids and lyophilization on the characteristics of eugenol-loaded liposomes prepared by ethanol injection method. *Food Biosci.* 2016;15:1-10. doi: 10.1016/j.fbio.2016.04.005
6. Guimarães D, Cavaco-Paulo A, Nogueira E. Design of liposomes as drug delivery system for therapeutic applications. *Int J Pharm.* 2021;601:120571. doi: 10.1016/j.ijpharm.2021.120571
7. Shah S, Dhawan V, Holm R, Nagarsenker MS, Perrie Y. Liposomes: Advancements and innovation in the manufacturing process. *Adv Drug Deliv Rev.* 2020;154-155:102-122. doi: 10.1016/j.addr.2020.07.002

8. Skupin-Mrugalska P, Piskorz J, Goslinski T, Mielcarek J, Konopka K, Düzgüneş N. Current status of liposomal porphyrinoid photosensitizers. *Drug Discov Today.* 2013;18(15-16):776-784. doi: 10.1016/j.drudis.2013.04.003
9. Magdy S, Alaaeldin E, Fathalla, *et al.* Metformin-loaded ethosomes with promoted anti-proliferative activity in melanoma cell line B16, and wound healing aptitude: Development, characterization and *in vivo* evaluation. *Int J Pharm.* 2022;621:121781. doi: 10.1016/j.ijpharm.2022.121781
10. Ashtikar M, Nagarsekar K, Fahr A. Transdermal delivery from liposomal formulations - Evolution of the technology over the last three decades. *J Control Release.* 2016;242:126-140. doi: 10.1016/j.jconrel.2016.09.008
11. Fang YP, Tsai YH, Wu PC, Huang YB. Comparison of 5-aminolevulinic acid-encapsulated liposome versus ethosome for skin delivery for photodynamic therapy. *Int J Pharm.* 2008;356(1-2):144-152. doi: 10.1016/j.ijpharm.2008.01.020
12. Fu X, Shi Y, Wang H, *et al.* Ethosomal gel for improving transdermal delivery of thymosin β-4. *Int J Nanomedicine.* 2019;14:9275-9284. doi: 10.2147/ijn.s228863
13. Mbah CC, Builders PF, Attama AA. Nanovesicular carriers as alternative drug delivery systems: Ethosomes in focus. *Expert Opin Drug Deliv.* 2014;11(1):45-59. doi: 10.1517/17425247.2013.860130
14. Paiva-Santos AC, Silva AL, Guerra C, *et al.* Ethosomes as nanocarriers for the development of skin delivery formulations. *Pharm Res.* 2021;38(6):947-970. doi: 10.1007/s11095-021-03053-5
15. Loginova AG, Nikitenko IS, Tikhonovsky GV, Skobeltsin AS, Voitova AV, Loschenov VB. Development of a method for assessing the depth of penetration of ethosomes with methylene blue into the skin during application and photodynamic exposure. *Biomed Photonics.* 2022;11(4):11-18. doi: 10.24931/2413-9432-2022-11-4-11-18
16. Shiryaev A, Ivankov M, Voitova A, *et al.* Photodynamic therapy under diagnostic control of wounds with antibiotic-resistant microflora. *Photonics.* 2024;11(7):594. doi: 10.3390/photonics11070594
17. Reshetov IV, Shiryaev AA, Vojtova AV, *et al. Method of Treating Purulent Wounds of Soft Tissues.* [Patent RU2836268C¹; 2025.
18. Kudryavtsev OS, Romshin AM, Pasternak DG, Vlasov II. Vacuum technique of nanodiamond dispersing on a substrate from an aqueous suspension. *J Vac Sci Technol B.* 2023;41(4):042805. doi: 10.1116/6.0002629
19. Limongi T, Susa F, Marini M, *et al.* Lipid-based nanovesicular drug delivery systems. *Nanomaterials (Basel).* 2021;11(12):3391. doi: 10.3390/nano11123391
20. Dahri M, Beheshtizadeh N, Seyedpour N, *et al.* Biomaterial-based delivery platforms for transdermal immunotherapy. *Biomed Pharmacother.* 2023;165:115048. doi: 10.1016/j.biopha.2023.115048
21. You DG, Yoon HY, Jeon S, *et al.* Deep tissue penetration of nanoparticles using pulsed-high intensity focused ultrasound. *Nano Converg.* 2017;4(1):30. doi: 10.1186/s40580-017-0124-z
22. Johnson PG, Gallo SA, Hui SW, Oseroff AR. A pulsed electric field enhances cutaneous delivery of methylene blue in excised full-thickness porcine skin. *J Invest Dermatol.* 1998;111(3):457-463. doi: 10.1046/j.1523-1747.1998.00301.x
23. Hood RR, Kendall EL, Junqueira M, *et al.* Microfluidic-enabled liposomes elucidate size-dependent transdermal transport. *PLoS One.* 2014;9(3):e92978. doi: 10.1371/journal.pone.0092978

Received: September 11, 2025
Revised: December 30, 2025
Accepted: March 11, 2026
Available online: May 13, 2026